separations

Article

Synthesis of Zeolitic Imidazolate Framework-8 from Waste Electrodes via Ball Milling for Efficient Uranium Removal

Minhua Su [1,†], Jinyao Zhu [1,†], Ruoning Wu [2], Jiaqi Pan [1], Jingran Yang [1], Jiaxue Zhao [1], Diyun Chen [1], Changzhong Liao [3], Kaimin Shih [4] and Shengshou Ma [4,*]

[1] School of Environmental Science and Engineering, Guangzhou University, Guangzhou 510006, China; teave@e.gzhu.edu.cn (J.P.); y19545627487@163.com (J.Y.); z1348044493@163.com (J.Z.); cdy@gzhu.edu.cn (D.C.)
[2] Shandong Key Laboratory of Water Pollution Control and Resource Reuse, School of Environmental Science and Engineering, Shandong University, Qingdao 266000, China; wrn1222@163.com
[3] State Key Laboratory of Featured Metal Materials and Life-Cycle Safety for Composite Structures, MOE Key Laboratory of New Processing Technology for Nonferrous Metals and Materials, School of Resources, Environment and Materials, Guangxi University, Nanning 530004, China; liaocz29@connect.hku.hk
[4] Department of Civil Engineering, The University of Hong Kong, Hong Kong SAR, China; kshih@hku.hk
* Correspondence: mass28@connect.hku.hk
† These authors contributed equally to this work.

Abstract: Developing a cost-effective approach for the remediation of wastewater containing uranyl [U(VI)] ions is essentially important to ecosystems and human health. In this study, a Zn-based ZIF-8 framework was fabricated from wasted batteries through an environmentally friendly ball milling process featuring a distinct microstructure compared to those synthesized from commercial Zn(II) sources. The as-obtained Zn-based ZIF-8 framework can effectively remove U(VI) ions from water, and a high removal efficiency of up to 99% is achieved across different process parameters, including initial dosage, pH values, and the presence of interfering ions. The superior U(VI) removal performance is attributed to the synergistic effect of microstructural features (e.g., crystallite size, specific surface area and pore diameter) and chemical interaction within the framework of Zn-based ZIF-8, resulting in the formation of the U···N chelates. This study integrates waste upcycling and hazardous U(VI) removal in an environmentally sound way, thereby promoting a circular economy.

Keywords: uranium removal; ZIF-8; ball milling; waste upcycling; circular economy

check for updates

Academic Editor: Dimosthenis Giokas

Received: 30 November 2024
Revised: 10 January 2025
Accepted: 26 January 2025
Published: 6 February 2025

Citation: Su, M.; Zhu, J.; Wu, R.; Pan, J.; Yang, J.; Zhao, J.; Chen, D.; Liao, C.; Shih, K.; Ma, S. Synthesis of Zeolitic Imidazolate Framework-8 from Waste Electrodes via Ball Milling for Efficient Uranium Removal. *Separations* **2025**, *12*, 40. https://doi.org/10.3390/separations12020040

Copyright: © 2025 by the authors. Licensee MDPI, Basel, Switzerland. This article is an open access article distributed under the terms and conditions of the Creative Commons Attribution (CC BY) license (https://creativecommons.org/licenses/by/4.0/).

1. Introduction

Nuclear energy plays an important role in the advancement of sustainable development. Uranium (U), a dominant nuclear fuel, has a high concentration in the continental crust [1]. Uranium exhibits various oxidation states in nature, such as +2, +3, +4, +5, and +6. The hexavalent state, U(VI), is the most stable and abundant form, with high toxicity. U(VI) typically exists as the uranyl ion (UO_2^{2+}), and its species distribution in aqueous solutions as a function of pH is shown in Figure 1. The inhalation of U(VI)-bearing particles can induce radiation damage to the lungs, potentially leading to lung cancer [2]. While U resources are essential for the operation of nuclear energy, the extraction of U from ores via mining and milling processes can generate large amounts of wastewater containing highly toxic hexavalent uranyl [U(VI)] ions [3]. Improper treatment of this wastewater can lead to severe environmental pollution and cause irreversible damage to human health [4,5].

Thus, it is imperative to develop reliable and efficient methods to alleviate the impact of uranium pollution.

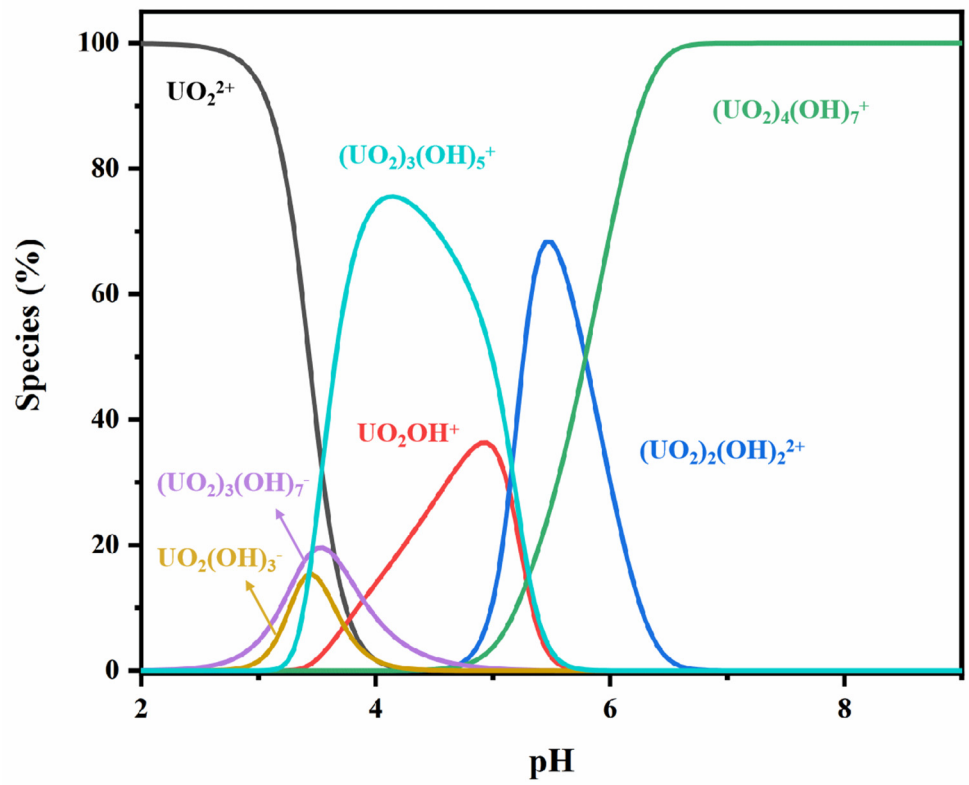


Figure 1. The species distribution of U(VI) as a function of pH value (precipitation conditions ($C(UO_2^{2+})$ = 20 ppm, calculated using Visual MINTEQ 3.1).

Chemical precipitation [6], ion exchange [7], membrane separation [8], and adsorption [9] are common practices in uranium-containing waste management. The chemical precipitation method utilizes chemical pH adjusters, such as NaOH, $Ca(OH)_2$, and CaO, to convert the U(VI) ions into insoluble uranium hydroxide precipitates for further separation [10]. However, the chemical precipitation process is highly dependent on the solution environment. The coexistence of other ions may adversely impact U precipitation efficiency [11]. The ion exchange method, which uses resins for U removal via a physical–chemical treatment, shows high U(VI) removal efficiency. Yet, it is limited by resin deactivation, leading to reduced lifetime and higher operation costs [7]. Membrane separation methods, such as reverse osmosis (RO), can process a large volume of uranium-containing wastewater and are easily scalable, but they suffer from high energy consumption, cost, complex processes, and membrane fouling [12]. Adsorption has been widely recognized as the most effective method for the removal of uranium owing to its high removal efficiency, easy handling, and less secondary pollution [13,14].

A variety of materials, such as graphene oxide (GO), nanofiber magnetic polymers (NMPs), and metal–organic frameworks (MOFs), have been investigated and used to remove uranium from wastewater streams. During the oxidation process of GOs, the π bonds in the graphene layer are destroyed, causing graphene oxide to lose its electrical conductivity and have structural disadvantages [15]. MNPs are a promising class of adsorbent materials due to their high biocompatibility, tunable functionality, and simple functionalization [16]. Fe_3O_4 is the most used magnetic material in the field of wastewater treatment. However, Fe_3O_4 particles tend to aggregate due to their huge specific surface

energy and internal magnetic attraction, which limits their application in separating and repairing metal ions.

Magnetic materials offer the advantage of facile separation from water using simple magnetic methods. However, their magnetic properties can also lead to agglomeration, potentially hindering their adsorption performance. To address this, Wang et al. (2023) developed a magnetic silica nanocomposite material ($NiFe_2O_4$@SiO_2@CS-PBTCA) based on chitosan for efficient U(VI) removal [17]. This material exhibited an impressive adsorption capacity of 125.30 $mg \cdot g^{-1}$ at pH 5.0, demonstrating good selectivity and recyclability. Polymer hybrids have shown great promise in uranium adsorption due to their high capacities. However, their preparation often involves complex multi-step syntheses and intricate surface modifications, increasing production costs and operational complexity. To overcome these challenges, Li et al. (2023) developed PAN-PC, a novel uranium adsorbent that achieves exceptional uranium adsorption through self-assembly [18]. By densely functionalizing PAN fibers with phosphocholine groups, PAN-PC surpasses the traditional 1:1 uranium/ligand stoichiometry, achieving a remarkable adsorption capacity of 2658 $mg \cdot g^{-1}$, with a stoichiometric ratio exceeding 5:1.

MOFs are porous materials formed by the coordination bonds between metals (or metal clusters) and organic ligands [19]. MOFs have become popular materials in adsorption applications due to their extremely high specific surface area, tunable pore structure, abundant unsaturated metal sites, and simple synthesis. Zeolitic imidazolate framework-8 (ZIF-8), a representative Zn-based MOF, has a large pore volume and surface area, reaching up to 0.85 $cm^3 \cdot g^{-1}$ and 1158 $m^2 \cdot g^{-1}$, respectively. It has demonstrated the ability to remove various pollutants, including heavy metals Cr(VI), Cu(II), and Pb(II), and antibiotics, such as norfloxacin tetracycline and oxytetracycline [20,21]. Its high thermal and chemical stability makes it suitable for a wide range of applications in diverse environments [22]. ZIF-8-bearing materials have been reported to effectively remove U(VI) ions. Their removal capabilities are summarized in Table 1. ZIF-8 is readily synthesized by coordinating Zn(II) and 2-methylimidazole. The Zn(II) precursor could be derived from multiple sources, including $Zn(NO_3)_2 \cdot 6H_2O$, $ZnCl_2$, $(CH_3COO)_2Zn$), and ZnO, and the choice of Zn(II) precursor varies with the synthetic method [23]. Common synthetic routes to ZIF-8 are solvothermal in the organic solvents of dimethylformamide (DMF) and methanol (MeOH), the microwave-assisted method, and mechanochemical [24]. Solvothermal and microwave-assisted processes rely heavily on organic solvents, leading to significant secondary pollution [25]. In addition, the use of Zn(II) salts, such as $Zn(NO_3)_2 \cdot 6H_2O$, could also result in problematic by-products. The mechanochemical process (i.e., ball milling) for ZIF-8 synthesis, using ZnO as a Zn(II) source and minimum organic solvent, can significantly reduce the carbon footprint and environmental pollution [26,27]. Commonly used zinc–manganese dry batteries contain considerable quantities of Zn source, which is overlooked and discarded. Such a valuable Zn source could be used as the secondary raw material for the synthesis of ZIF-8, further improving environmental sustainability. This work presents an eco-friendly process for the conversion of waste electrodes derived from spent dry batteries into ZIF-8 products. The adsorption performance of the obtained ball-milled ZIF-8 and other ZIF-8 samples synthesized from commercial Zn(II) sources for uranium removal from simulated wastewater was evaluated under different process conditions, providing a basis for future practical implementation. This work explores the potential of waste battery material for the synthesis of ZIF-8 via a green route, demonstrating its comparable U(VI) removal performance to the ZIF-8 synthesized from commercial raw material. This research contributes to the development of sustainable and environmentally friendly solutions for waste management.

Table 1. A comparison of similar materials.

Material	Method	Removal (%)	Specific Surface Area (m^2/g)	Pore Volume (cm^3/g)	Average Pore Diameter (nm)	Ref.
chitosan/ ZIF-8/algal powder	hydrothermal method	89	3.645	0.052	57.210	[28]
ZIF-8-CN	one-pot method		308.17	0.35	4.59	[29]
ZIF-8/PAO	solvent-induced phase separation method	99	386.54	2.55	0.2464	[30]
H-PDA/SA-ZIF-8	controlled etching process		1234.924	0.68		[31]
CO/ZIF-8@SA		90				[32]

2. Materials and Methods

2.1. Materials and ZIF-8 Synthesis

The flowchart in Figure 2 outlines the process involved in the preparation of three ZIF-8 samples C-AQ, W-BM, and C-BM. Sample C-AQ was synthesized via an aqueous solution route adopted from a previously reported procedure [27,33]. To be exact, 0.74 g of $Zn(NO_3)_2 \cdot 6H_2O$ (98%, Sigma-Aldrich, USA) and 12.28 g of 2-methylimidazole (Hmim, 99%, ACROS, Belgium) were separately dissolved in 10 mL and 90 mL of deionized (DI) water, and the two solutions were mixed gradually. The resulting mixture was stirred for 3 h at room temperature to form a white, milky suspension. After filtration with a 0.22 µm pore-size membrane filter, the collected solid was washed with methanol three times and then dried in a furnace at 50 °C overnight. Samples W-BM and C-BM were synthesized using a solvent-less mechanochemical process, differing only in the input of metal sources (waste ZnO extracted from discarded batteries for W-BM and commercial ZnO for C-BM), while all other conditions were kept identical. In this process, 0.497 g of waste/commercial ZnO and 1.5033 g of Hmim were added to a 50 mL zirconia milling container. Zirconia balls and 2 mL of methanol (99.6%, Sigma-Aldrich) were employed to facilitate the reaction. The reaction was commenced at 500 rpm for 10 h. The obtained pasty samples were collected and washed three times using 50 mL of deionized water and dried in a furnace at 60 °C overnight.

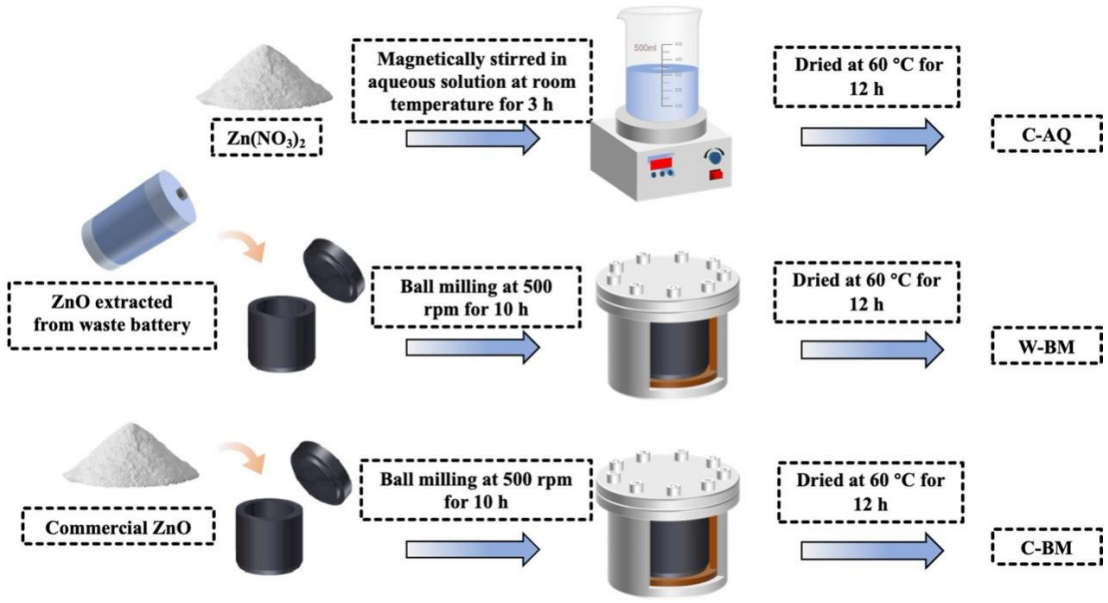


Figure 2. Flowchart illustrating three experimental processes for the preparation of ZIF-8.

2.2. Batch Adsorption Experiments

A uranium stock solution (in the form of UO_2^{2+}) with a concentration of 1000 ppm was prepared by dissolving uranium salt in deionized water, and it was stabilized by adding concentrated nitric acid (HNO_3). Experiments for the adsorption of U(VI) by ZIF-8 samples were conducted in a beaker positioned on the temperature-controlled magnetic stirrer at room temperature (25 ± 1 °C). The reaction time was set between 0.5 and 90 min, sampling at each time interval. In addition, other parameters, including pH (3–8), sample dosage (0.2–1.0 g·L^{-1}), initial concentration of U(VI) (20–60 ppm), and interfering metal ions (Na^+, Mg^{2+}, K^+, and Ga^{2+}), were also examined for the removal of U(VI) by the synthesized ZIF-8. During the adsorption experiment process, ZIF-8 samples were added into a beaker containing 30 mL of uranium solution, and the pH was tuned using 0.1 M of HNO_3 and NaOH. The reaction was commenced with a magnetic stirring speed of 600 rpm. At each sampling interval, the mixtures were filtered with a 0.45 μm pore-size water-based filter. The U(VI) concentrations in the resulting solution were analyzed using an ultraviolet-visible (UV-Vis) spectrophotometer (UV-1900i; Japan). The adsorption capacity and adsorption efficiency of ZIF-8 for U(VI) were calculated using Equations (1) and (2), respectively:

$$\text{Adsorption capacity} = \frac{(C_t - C_o)V}{m} \quad (1)$$

$$\text{Removal efficiency}(\%) = \frac{C_t - C_o}{m} \times 100\% \quad (2)$$

where C_0 (mg·L^{-1}), C_t (mg·L^{-1}), m (g), and V (L) are the initial concentration of U(VI), the remaining U(VI) concentration in the solution, and the quality of ZIF-8 and solution volume, respectively.

2.3. Material Characterization

Phase components were determined via X-ray diffraction (XRD) analysis. The XRD data were collected using a Bruker D8 Advance diffractometer equipped with a Cu Kα radiation source (λ = 1.5418 Å). The morphology of the synthesized samples was observed using a scanning electron microscope (SEM, Hitachi S-4800, Japan) after gold sputtering. The N_2 physisorption analyses and measurements of the specific surface areas and pore diameters were performed at a liquid nitrogen temperature (77 K) using an Anton par Autosorb 6100 high-pressure gas sorption analyzer. Prior to BET measurement, the samples were degassed at 200 °C for 8 h. The samples were analyzed by Fourier transform infrared (FTIR) spectroscopy (PerkinElmer Spectrum 100 spectrometer) using the KBr pellet method. The surface valence of the samples (XPS) was analyzed using a Thermo Scientific™ ESCALAB™ Xi^+ X-ray Photoelectron Spectrometer. A list of the instrument models and their places of origin used in this work is provided in Table 2.

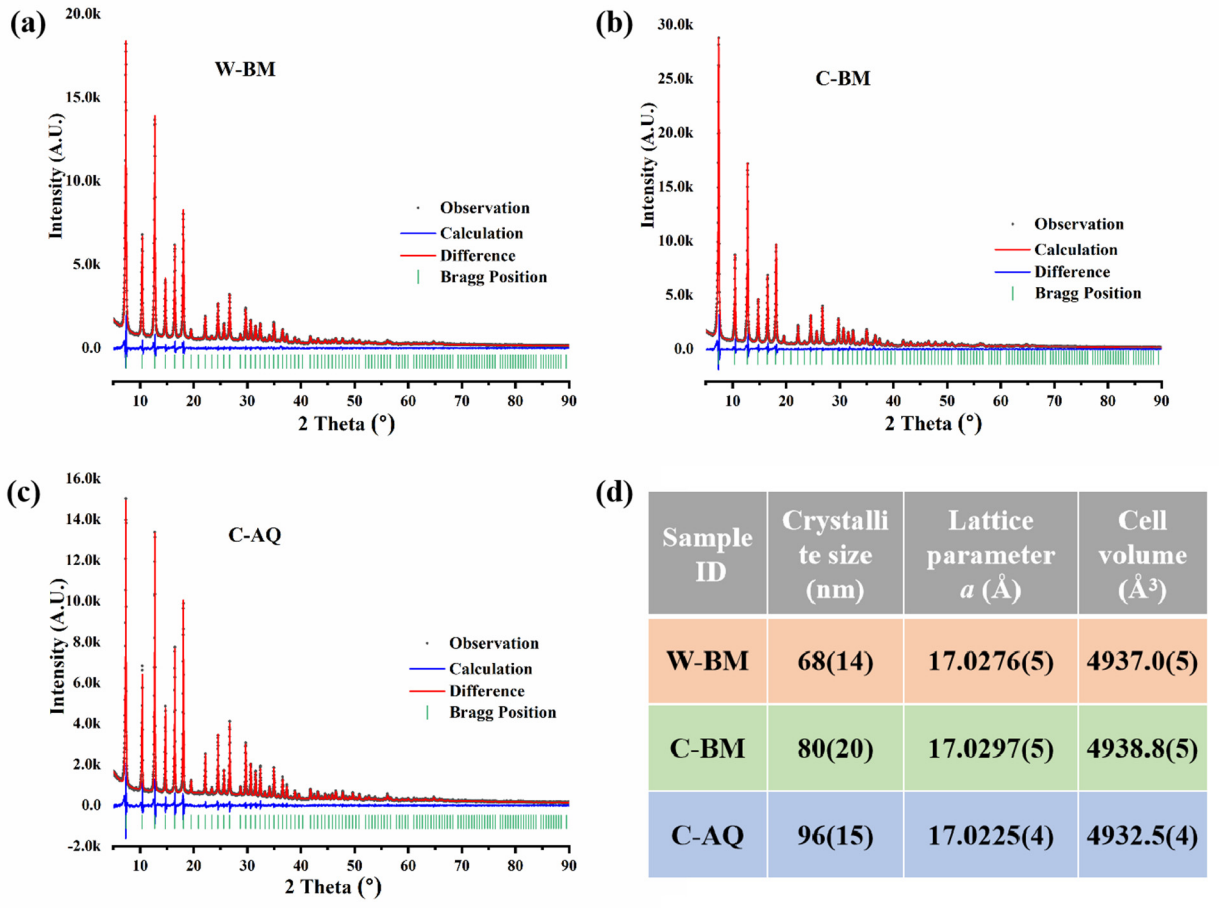
Table 2. List of analytical instruments.

Characterize	Model	Country
FTIR	PerkinElmer Spectrum100	America
XRD	Bruker D8 Advance	Germany
BET	Autosorb 6100	America
SEM	Sigma 300+ UILTIM MAX	Britain
TEM	JEOL JEM 2100 F	Japan
XPS	Thermo Scientific ESCALAB Xi+	America

3. Results and Discussion

3.1. Characterization of ZIF-8

Figure 3a–c show the XRD patterns of ZIF-8 prepared via a ball milling route and from an aqueous solution. The three synthesized samples featured similar XRD peak positions that can be indexed as a ZIF-8 structure with a sodalite topology (CCDC 1046832). Nevertheless, the XRD peak profiles among these ZIF-8 samples exhibited subtle differences, suggesting the microstructural features (e.g., crystallite sizes and morphology) of these ZIF-8 samples differ slightly. The Pawley refinement method was carried out to quantify the differences based on the XRD data. The Pawley refinement provided a satisfactory fit to the experimental data. The crystallite sizes of W-BM, C-BM, and C-AQ were estimated to be 68(40) nm, 80(20) nm, and 96(15) nm, respectively, indicating a much smaller crystallite size of ZIF-8 synthesized from the waste electrodes. The lattice parameter *a* and cell volume for samples W-BM, C-BM, and C-AQ were determined to be 17.0276(5) Å, 17.0297(5) Å, 17.0225(4) Å, and 4937.0(5) $Å^3$, 4938.8(5) $Å^3$, 4932.5(4) $Å^3$, respectively. These findings demonstrate ZIF-8 synthesized from different routes exhibiting an identical crystalline phase while showing slight variations in its microstructural features.



Sample ID	Crystallite size (nm)	Lattice parameter *a* (Å)	Cell volume ($Å^3$)
W-BM	68(14)	17.0276(5)	4937.0(5)
C-BM	80(20)	17.0297(5)	4938.8(5)
C-AQ	96(15)	17.0225(4)	4932.5(4)

Figure 3. (**a**) Pawley-refined XRD patterns of sample W-BM; (**b**) Pawley-refined XRD patterns of sample C-BM; (**c**) Pawley-refined XRD patterns of sample W-BM; (**d**) refined crystallite size, lattice parameter, and cell volume of three ZIF-8 samples W-BM, C-BM, and C-AQ.

The nitrogen adsorption–desorption patterns (Figure 4a) reveal type IV isotherms, indicating that the ZIF-8 samples C-AQ, W-BM, and C-BM feature a porous structure, which is consistent with the reported ZIF-8 structure. In addition, W-BM synthesized from waste ZnO exhibited a significantly higher specific surface area of 1433.94 $m^2 \cdot g^{-1}$ and a larger pore diameter of 7.86 nm compared to the two ZIF-8 samples C-AQ (981.26 $m^2 \cdot g^{-1}$ and

3.07 nm) and C-BM (1031.93 $m^2 \cdot g^{-1}$ and 3.69 nm), which were synthesized from commercial zinc sources via an aqueous solution route and a ball milling process. The higher specific surface area of W-BM is attributed to its smaller crystallite size compared to the two ZIF-8 samples, C-AQ and C-BM. The larger surface area might offer more active sites for the reaction. Figure 4c shows that three ZIF-8 samples, C-AQ, W-BM, and C-BM, have nearly identical FTIR spectra. Consequently, the vibrational analysis was based on a single ZIF-8 sample. The most typical characteristic peaks are associated with the vibration of imidazole. For instance, the bands at 3622 and 2930 cm^{-1} were ascribed to the C-H stretching of methyl groups [27,34]. The peaks at 1306 and 752 cm^{-1} were associated with the entire imidazole ring vibration mode, and 1178 and 1146 cm^{-1} were assigned to C–N stretches [35,36]. The characteristic peak at 420 cm^{-1} belonging to Zn–N bonds was also observed, confirming the successful synthesis of ZIF-8. The SEM images (Figure 4d,e) show the difference in morphologies and crystallites of ZIF-8 samples W-BM and C-AQ synthesized via two distinct methods. The former exhibited irregular morphologies and aggregated particles in contrast to the well-dispersed, regular morphology of the latter.

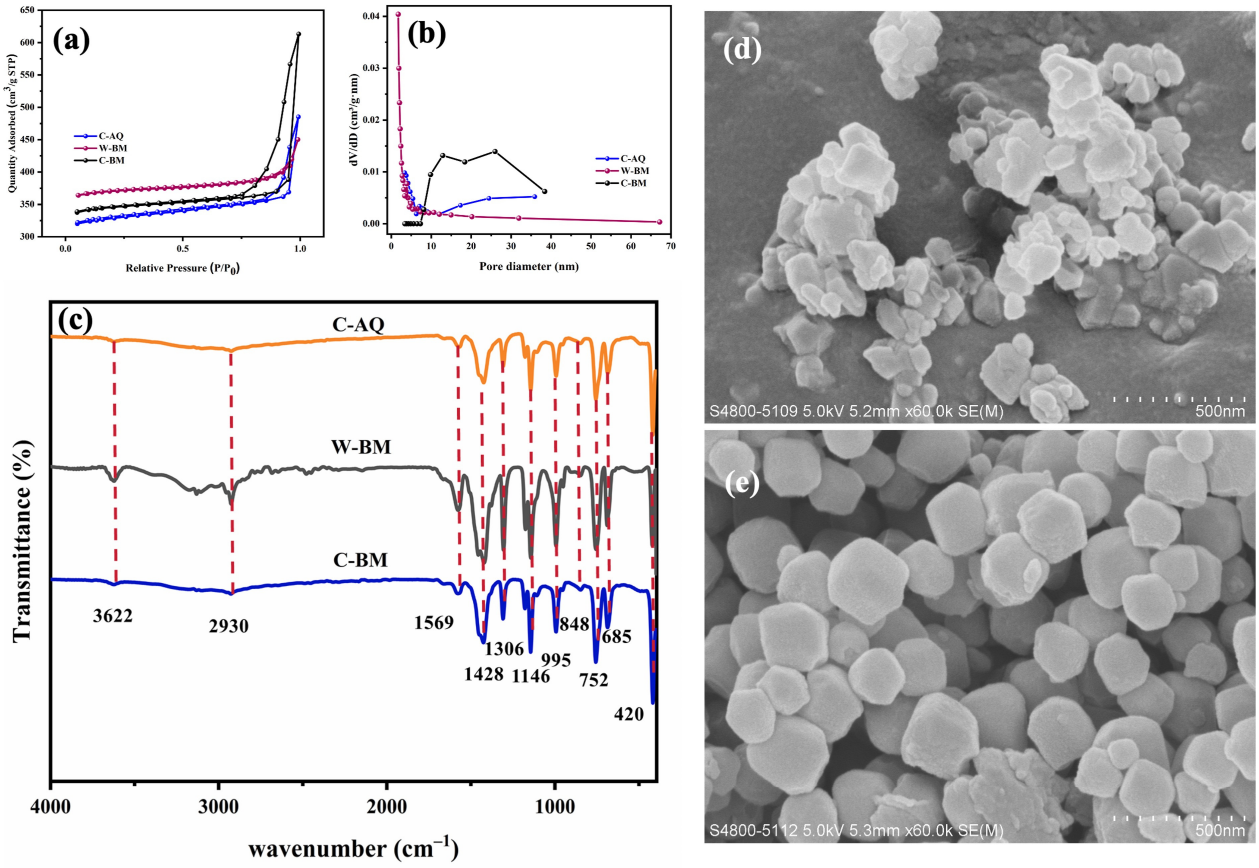


Figure 4. (**a**) N_2 adsorption/desorption isotherm of ZIF-8 samples C-AQ, W-BM, and C-BM; (**b**) pore-size distributions of ZIF-8 samples C-AQ, W-BM, and C-BM; (**c**) FTIR patterns of ZIF-8 samples C-AQ, W-BM, and C-BM; (**d**) SEM image of W-BM at 500 nm scale; (**e**) SEM image of C-AQ at 500 nm scale.

3.2. U(VI) Absorption Performance of ZIF-8

Prior to evaluating the U(VI) adsorption performance of the synthesized ZIF-8, control experiments were performed to analyze the U(VI) concentration variations in a uranium solution without ZIF-8 under different pH conditions (Figure 5a). During the initial 2 h shaking period, the U(VI) concentration remained insignificant, while the concentration showed a reduction at both pH = 7 and pH = 9, with a significant reduction

observed at pH = 9, after a 1-day standing period. This suggests that the precipitation of U(VI) is less likely within 2 h. Higher pH conditions and extended standing times (>2 h) can facilitate precipitation. Thus, the variation in the U(VI) concentration in the solution containing ZIF-8 is not theoretically influenced by precipitation. The ZIF-8 samples C-AQ, C-BM, and W-BM were subjected to experiments to analyze the effects of contact time, pH, and dosage on U(VI) removal. The adsorption kinetics experiments show that U(VI) was rapidly removed by the three ZIF-8 samples at the beginning of adsorption, with the highest removal efficiency for W-BM, followed by C-BM and C-AQ. The removal efficiency gradually increases until adsorption equilibrium is reached at around 20 min for W-BM, 30 min for C-BM, and 60 min for C-AQ, respectively (Figure 5b). It should be noted that the removal efficiency for W-BM reaches nearly 100% at equilibrium, indicating that ZIF-8 synthesized from waste ZnO exhibits remarkable U(VI) adsorption capability. The influence of solution pH on the removal efficiency of U(VI) was evaluated for the three ZIF-8 samples. Over an initial pH range of 3 to 8, three synthesized ZIF-8 samples exhibited high U(VI) removal efficiencies (Figure 5c). Notably, sample W-BM achieved near complete removal of U(VI) under the tested pH conditions. Figure 5d shows that increasing the dosage of ZIF-8 did not result in a significant improvement in U(VI) removal efficiency. Nevertheless, all three ZIF-8 samples showed high removal efficiencies, with W-BM consistently achieving the highest removal efficiencies within the dosage range. Thus, the ZIF-8 samples, particularly those synthesized from waste ZnO, exhibited superior removal capability for U(VI) ions across a range of contact times and pH conditions.

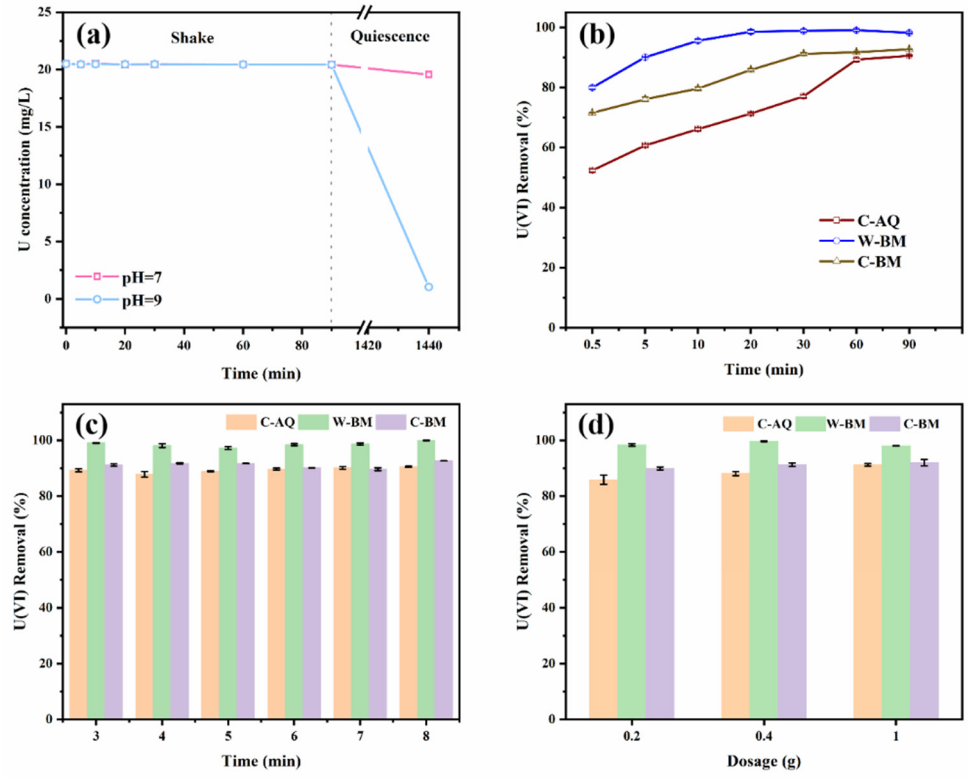


Figure 5. (**a**) Precipitation of U(VI) solution at different pH values; (**b**) time-dependent removal of U in samples C-AQ, W-BM, and C-BM; (**c**) initial pH-dependent removal of U(VI) in samples C-AQ, W-BM, and C-BM; (**d**) the effect of the initial dosage of samples C-AQ, W-BM, and C-BM on U(VI) removal.

To further investigate the U(VI) adsorption performance of ZIF-8 synthesized from waste ZnO via a ball milling process (W-BM), the effects of process parameters, including initial U(VI) concentration, contact time, dosage, pH, and interfering ions, on the removal

efficiencies were evaluated. Figure 6a shows that W-BM demonstrated rapid removal of U(VI), with a high removal efficiency achieved within the first minute, especially at lower initial U(VI) concentrations (20 ppm). Also, at this initial concentration, the adsorption equilibrium of U(VI) was attained within 20 min. As the initial U(VI) concentration increased from 20 to 60 ppm, the time to reach adsorption equilibrium was prolonged. Figure 6b illustrates that U(VI) removal efficiencies were not significantly affected by increasing the dosage of W-BM, indicating that a high level of U(VI) removal efficiency can still be achieved even with a small amount of W-BM. The U(VI) adsorption capacity exhibited a decreasing trend as the dosage increased, which is likely due to the saturation of active sites on the ZIF-8 surface.

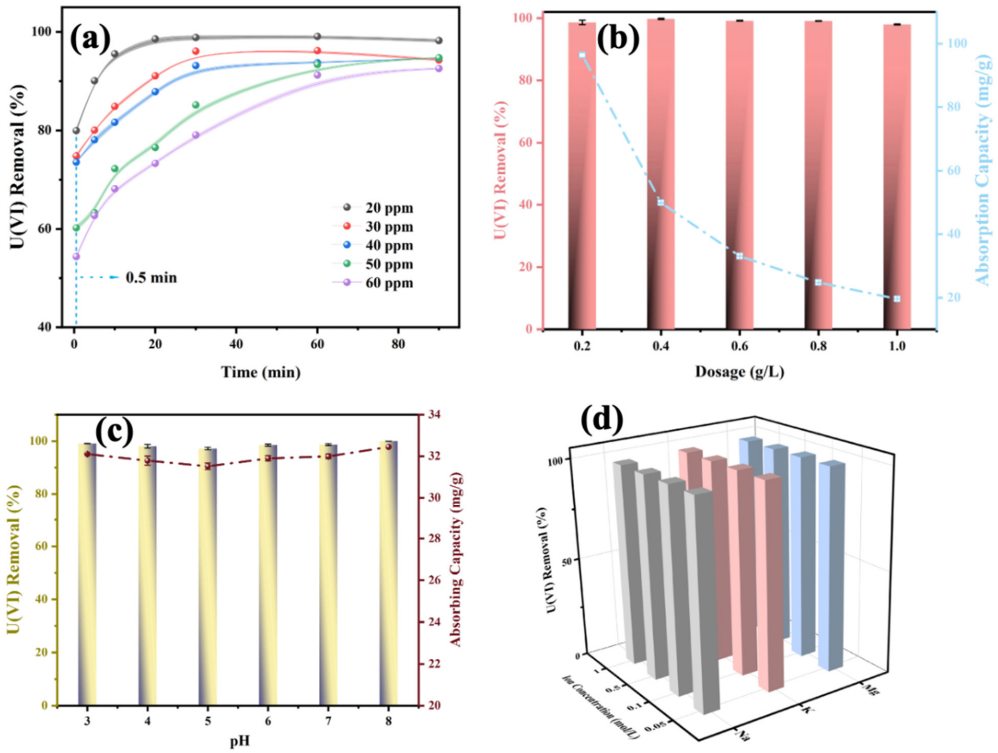


Figure 6. (**a**) Effect of contact time and initial U(VI) concentration on U(VI) removal efficiency; (**b**) effect of dosage on U(VI) removal efficiency and adsorption capacity; (**c**) effect of initial pH on U(VI) removal efficiency and adsorption capacity (c(U(VI)) = 20 ppm, dosage = 0.6 g·L^{-1}); (**d**) U(VI) removal in the presence of Na^+, K^+, and Mg^{2+}.

The effect of initial pH on the U(VI) removal efficiency and adsorption capacity of W-BM was also studied (Figure 6c). Over the initial pH range, sample W-BM exhibited high U(VI) removal efficiencies, approaching complete elimination. Three replicate experiments were performed, and the average U(VI) removal efficiency was found to be 97.83%. A one-sample t-test was performed on the removal efficiencies to assess variability. With a *p*-value of 0.215, the results indicate no statistically significant difference between the replicates. This suggests that within the experimental conditions, variations in pH had a negligible effect on the adsorption performance of W-BM, demonstrating its relative stability under these conditions. The impact of interfering cations, including Mg^{2+}, K^+, and Na^+, on the U(VI) adsorption by ZIF-8 was also explored because these ions are prevalent in natural water sources. Figure 6d shows that the U(VI) removal efficiencies were maintained at a high level of 99% in the presence of Mg^{2+}, K^+, Na^+, and the ZIF-8 sample W-BM. Moreover, even at high concentrations, these interfering cations have a limited inhibitory effect on U(VI) removal, indicating ZIF-8 synthesized from waste ZnO is highly effective in

reducing the concentration of U(VI) in natural water sources. This suggests that ZIF-8 has a significant potential advantage in treating real wastewater containing U(VI).

Batch experiments demonstrate that the ZIF-8 sample W-BM, synthesized from waste ZnO, possessed superior U(VI) removal capacity. To further investigate the adsorption behavior of U(VI) on W-BM, Langmuir and Freundlich isothermal adsorption models were adopted to fit the experimental data. Langmuir isotherm is more suitable for monolayer adsorption on homogeneous sites, whereas Freundlich isotherm is better suited for multilayer adsorption on heterogenous sites [37]. Equations (3) and (4) can be used to express the two models, respectively:

$$q_e = \frac{K_L q_m C_e}{1 + K_L C_e} \tag{3}$$

$$q_e = K_F C_e^{\frac{1}{n}} \tag{4}$$

where K_L and K_F are the isothermal equilibrium constants of the Langmuir model and the Freundlich model, respectively; n is the correlation coefficient for adsorption affinity; q_e and C_e are equilibrium adsorption capacity ($mg \cdot g^{-1}$) and equilibrium concentration ($mg \cdot L^{-1}$); and q_m is the maximum adsorption capacity ($mg \cdot g^{-1}$).

As depicted in Figure 7a and Table 3, the poor fitting results suggest that the Redlich–Peterson and Dubinin–Radushkevich models may not adequately describe the adsorption behavior in this work. Nevertheless, the Freundlich model (R^2 = 0.9702) showed better agreement with experimental data than the Langmuir model (R^2 = 0.8359), suggesting the adsorption of U(VI) onto the ZIF-8 sample W-BM is more likely to occur on heterogeneous sites rather than homogeneous sites. In other words, multilayer adsorption may be the primary adsorption mechanism, considering the porous structure of ZIF-8.

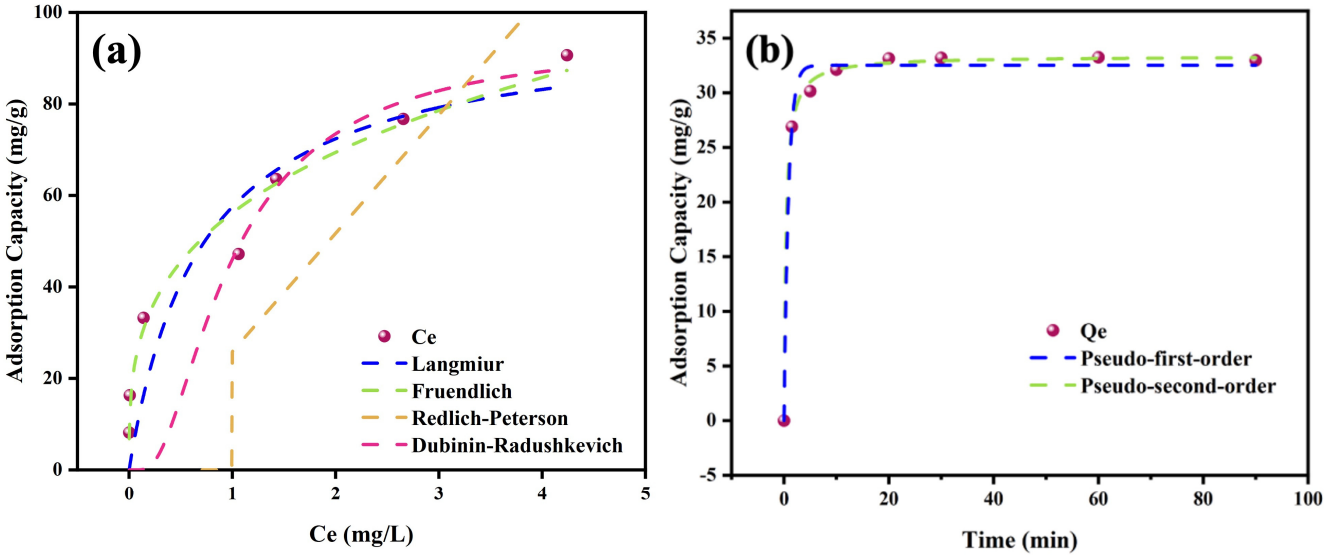


Figure 7. (**a**) Adsorption isotherms for U(VI) onto ZIF-8 sample W-BM; (**b**) pseudo-first-order kinetic model and pseudo-second-order kinetic model of U (VI) adsorption onto ZIF-8 sample W-BM.

On the other hand, the kinetic study of U(VI) adsorption on the ZIF-8 sample W-BM was performed. As shown in Figure 7b, the adsorption capacity of W-BM undergoes a sharp increase in the initial 10 min and then stabilizes. The maximum adsorption capacity in W-BM was approximately 32 $mg \cdot g^{-1}$. A pseudo-first-order reaction kinetic model and pseudo-second-order reaction kinetic model were fitted to the experimental data, and the equations are given as follows:

$$q_t = q_e\left(1 - e^{-k_1 t}\right) \tag{5}$$

$$q_t = \frac{k_2 q_e^2 t}{1 + k_2 q_e t} \quad (6)$$

where q_t is the adsorption capacity at t time (mg·g^{-1}); q_e is the adsorption capacity at equilibrium (mg·g^{-1}); and k_1 and k_2 are the adsorption rate constants of the pseudo-first-order reaction kinetic model and the pseudo-second-order reaction kinetic model, respectively. The calculated parameters are outlined in Table 3. The higher R^2 value (0.9986) for the pseudo-second-order model indicates that the adsorption of U(VI) onto ZIF-8 was primarily governed by the chemical adsorption process.

Table 3. Isotherm constants and kinetic parameters for U (VI) adsorption onto W-BM.

Langmuir Isotherm			**Freundlich Isotherm**		
q_m (mg·g^{-1})	K_L (L·mg^{-1})	R^2	K_F (L·mg^{-1})	$1/n$	R^2
97.58	1.4366	0.8359	56.1171	0.3053	0.9702
Redlich–Peterson			Dubinin–Radushkevich		
a	K_R	R^2	q_m (mg·g^{-1})	K_D	R^2
1×10^{-4}	25.8587	0.2170	93.68	1.4782	0.6924
Pseudo-first-order			Pseudo-second-order		
k_1 (min^{-1})	q_e (mg·g^{-1})	R^2	k_2 (L·mg^{-1})	q_e (mg·g^{-1})	R^2
1.1563	32.5100	0.9911	0.0792	33.3438	0.9986

3.3. Durability of W-BM for U(VI) Removal

The re-utility of materials is crucial for their practical application in water treatment. To evaluate the recyclability of W-BM, five consecutive adsorption–desorption cycles were conducted. As illustrated in Figure 8, W-BM maintained a U(VI) removal efficiency exceeding 80% even after five cycles, demonstrating its potential for sustainable use in water treatment processes.

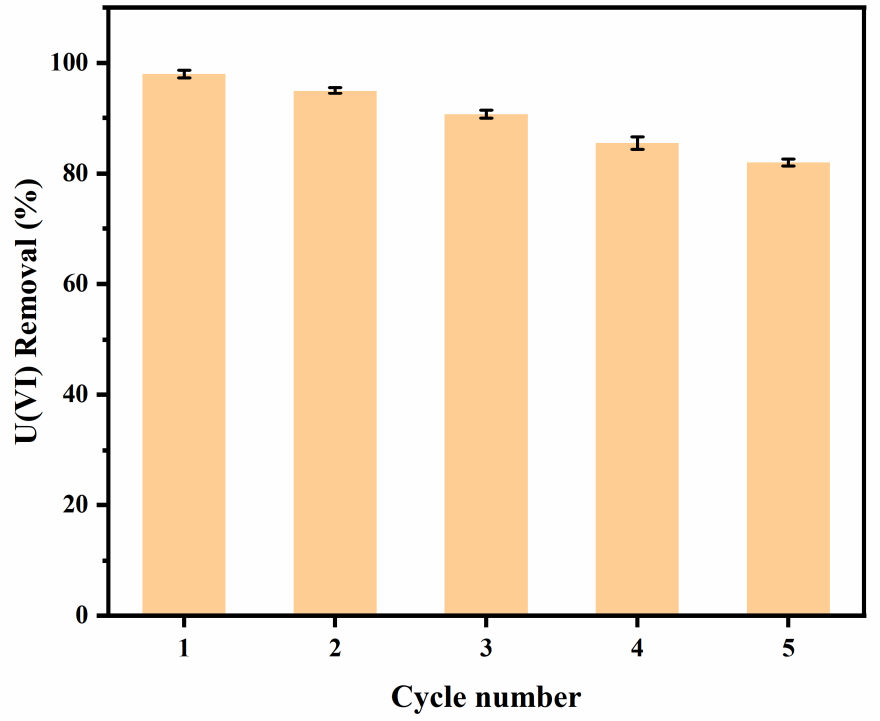


Figure 8. U(VI) removal efficiency of ZIF-8 during five cycles used.

3.4. Reaction Mechanism

In further investigating the adsorption mechanism, the ZIF-8 sample W-BM, synthesized from waste ZnO, was characterized for its elemental and structural properties. Figure 9 shows an SEM image of W-BM after U(VI) adsorption and the corresponding EDS mapping images. The homogenous dispersion of U(VI) within the ZIF-8 sample that contains Zn, C, and N suggests a high affinity between U and ZIF-8, leading to adsorption into the structure. Moreover, a significant reduction in the intensity of the XRD peaks was noted for the sample W-BM after adsorption (Figure 10a), indicating the adsorption of U(VI) resulted in a gradual loss of long-range order in the structure. The high-resolution XPS spectrum of W-BM after U(VI) reveals two U $4f_{5/2}$ and U $4f_{7/2}$ peaks at 392.5 eV and 381.9 eV, which can be attributed to the splitting of unpaired electrons, respectively [38]. This observation also suggests a strong interaction between W-BM and U(VI), resulting in the distribution of U(VI) on the ZIF-8 sample W-BM. While the loss of long-range order and the occurrence of U(VI) in the sample were observed, the high-resolution XPS spectra of Zn 2p showed little change in W-BM before and after U(VI) adsorption, implying that the adsorption of U(VI) did not affect the local environment around Zn. A comparison of the FTIR spectra of W-BM before and after U(VI) adsorption reveals that most vibrational modes, including the imidazole ring and the Zn–N bond, were retained, even with the loss of long-range order in the structure induced by the adsorption process. However, for the sample W-BM after U(VI) adsorption, a distinct peak (896 cm^{-1}) was noted among the imidazole ring vibrational bands. This observation suggests that U(VI) ions were preferentially adsorbed onto the imidazole ring of the ZIF-8 structure, consistent with a previous density functional theory study indicating bidentate chelation between U(VI) and N atoms in imidazole rings [39]. Therefore, the adsorption mechanism of U(VI) onto the ZIF-8 sample W-BM can be attributed to the chelate formation of U(VI) with N atoms from imidazole rings.

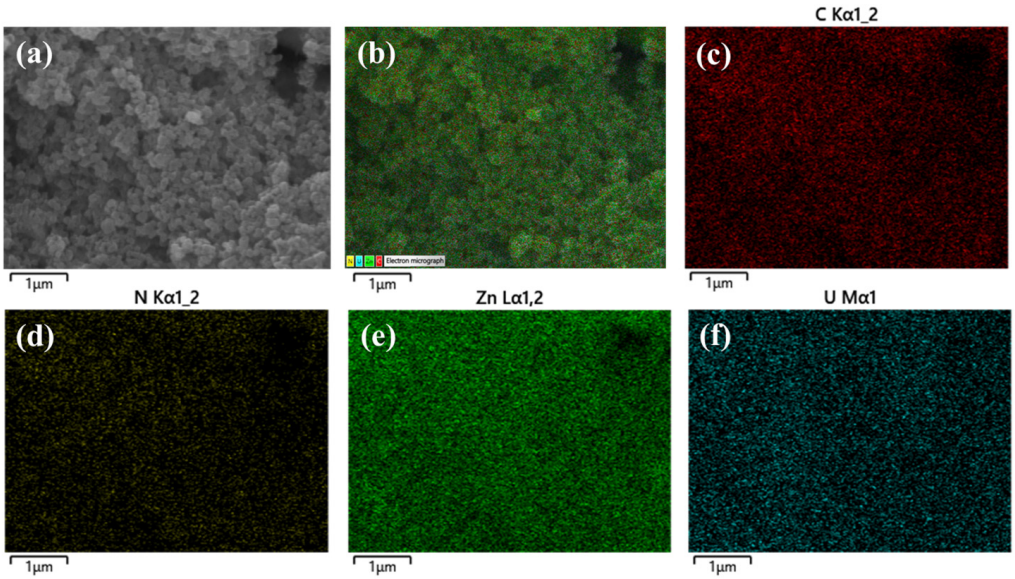


Figure 9. (**a**) SEM image of W-BM after U(VI) adsorption; (**b**) elemental mapping micrograph; (**c**) C elemental mapping image; (**d**) N elemental mapping image; (**e**) Zn elemental mapping image; (**f**) U elemental mapping image.

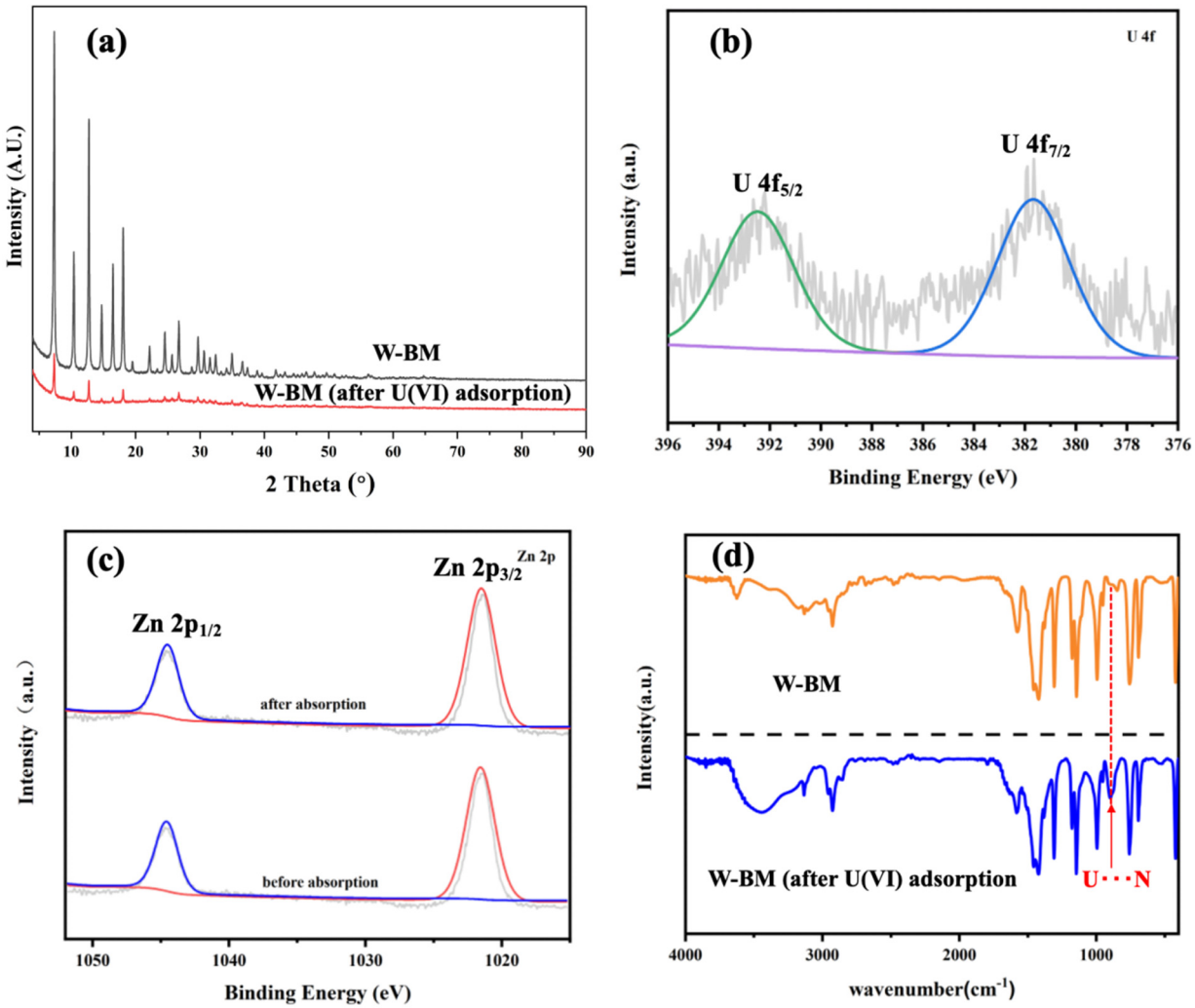


Figure 10. (**a**) XRD patterns of W-BM before and after U(VI) adsorption; (**b**) high-resolution XPS spectrum of U 4f (The purple line is the background signal; the green and blue lines are the fitting results, respectively); (**c**) high-resolution XPS spectra of Zn 2p in W-BM before and after adsorption (the blue and orange lines are the fitting results, respectively); (**d**) FTIR spectra of W-BM before and after U(VI) adsorption.

4. Conclusions

This study demonstrates a cost-effective approach to valorize waste electrode material by transforming it into ZIF-8 for U(IV) removal. ZIF-8 was successfully synthesized from waste ZnO derived from spent dry batteries through a mechanochemical process. Characterization techniques, including XRD, BET, FTIR, and SEM, revealed that ZIF-8 synthesized from waste ZnO (W-BM) exhibited a smaller crystallite size, a higher specific surface area, and a larger pore diameter compared to those synthesized from commercial Zn(II) sources. The batch experimental results confirm the effectiveness of the ZIF-8 sample W-BM in the removal of U(VI) ions from water, reaching near complete removal within a short equilibrium period, even in the presence of interfering alkaline ions Na^+, K^+, and Mg^{2+} and across various initial dosages and pH values. The kinetic study suggests that the adsorption of U(VI) onto ZIF-8 is primarily driven by a chemical adsorption process. The reaction mechanism may be explained by the chelate formation of U(VI) with N atoms from imidazole rings within the ZIF-8 structure. The utilization of waste ZnO extracted from discarded alkaline batteries at no cost offers a significant economic advantage compared to commercial ZnO (Sigma-Aldrich, reagent grade) (USD 51.52

per 100 g) and $Zn(NO_3)_2{\cdot}6H_2O$ (Sigma-Aldrich, reagent grade) (USD 31.26 per 100 g). Overall, this work provides a promising pathway to environmental sustainability and resource conservation.

Author Contributions: Conceptualization, M.S., R.W., K.S. and S.M.; Methodology, J.Z. (Jinyao Zhu), R.W., J.P., J.Y. and J.Z. (Jiaxue Zhao); Software, S.M.; Validation, J.Z. (Jinyao Zhu); Data curation, J.Z. (Jinyao Zhu), R.W., J.P., J.Y. and J.Z. (Jiaxue Zhao); Formal analysis, M.S. and S.M.; Investigation, J.Z. (Jinyao Zhu); Resources, M.S. and C.L.; Writing—original draft, R.W.; Writing—review & editing, M.S., D.C., C.L. and K.S.; Visualization, D.C. and K.S.; Supervision, S.M. All authors have read and agreed to the published version of the manuscript.

Funding: This work was supported by the National Natural Science Foundation of China (22076034, 42230719, and 22276043) and the Science and Technology Planning Project of Guangzhou City, China (2025A03J3090 and 2024A03J00314).

Data Availability Statement: Data is contained within the article.

Conflicts of Interest: The authors declare no conflict of interest.

References

1. Haack, U. On the content and vertical distribution of K, Th and U in the continental crust. *Earth Planet. Sci. Lett.* **1983**, *62*, 360–366. [CrossRef]
2. Hettiarachchi, E.; Das, M.; Cadol, D.; Frey, B.A.; Rubasinghege, G. The fate of inhaled uranium-containing particles upon clearance to gastrointestinal tract. *Environ. Sci. Process. Impacts* **2022**, *24*, 1257–1266. [CrossRef]
3. Ye, Y.; Jin, J.; Han, W.; Miao, S.; Feng, Y.; Qin, Z.; Tang, X.; Li, C.; Chen, Y.; Chen, F.; et al. Spontaneous electrochemical uranium extraction from wastewater with net electrical energy production. *Nat. Water* **2023**, *1*, 887–898. [CrossRef]
4. Tsarev, S.; Collins, R.N.; Fahy, A.; Waite, T.D. Reduced Uranium Phases Produced from Anaerobic Reaction with Nanoscale Zerovalent Iron. *Environ. Sci. Technol.* **2016**, *50*, 2595–2601. [CrossRef]
5. Zheng, M.; Ji, H.; Duan, J.; Dang, C.; Chen, X.; Liu, W. Efficient adsorption of europium (III) and uranium (VI) by titanate nanorings: Insights into radioactive metal species. *Environ. Sci. Ecotechnol.* **2020**, *2*, 100031. [CrossRef]
6. Du, M.; Hylton, T.D.; Robinson, S.M. Chemical processes for recovery and purification of high-purity uranium-234 from aged plutonium-238. *J. Radioanal. Nucl. Chem.* **2021**, *327*, 417–424. [CrossRef]
7. Chen, F.; Lv, M.; Ye, Y.; Miao, S.; Tang, X.; Liu, Y.; Liang, B.; Qin, Z.; Chen, Y.; He, Z.; et al. Insights on uranium removal by ion exchange columns: The deactivation mechanisms, and an overlooked biological pathway. *Chem. Eng. J.* **2022**, *434*, 134708. [CrossRef]
8. Zhou, C.; Ontiveros-Valencia, A.; Cyr, L.C.D.S.; Zevin, A.S.; Carey, S.E.; Krajmalnik-Brown, R.; Rittmann, B.E. Uranium removal and microbial community in a H_2-based membrane biofilm reactor. *Water Res.* **2014**, *64*, 255–264. [CrossRef]
9. Bone, S.E.; Dynes, J.J.; Cliff, J.; Bargar, J.R. Uranium(IV) adsorption by natural organic matter in anoxic sediments. *Proc. Natl. Acad. Sci. USA* **2017**, *114*, 711–716. [CrossRef]
10. Lee, H.K.; Chang, S.; Park, W.; Kim, T.J.; Park, S.; Jeon, H. Effective treatment of uranium-contaminated soil-washing effluent using precipitation/flocculation process for water reuse and solid waste disposal. *J. Water Process Eng.* **2022**, *48*, 102890. [CrossRef]
11. Gao, J.; Chen, J.; Lv, H.; Feng, X.; Liao, S.; Zhang, L.; Ma, F.; Xue, Y.; Ji, M.; Wang, H. Shielding process for the effect of anions on uranium selective recovery and heavy metal removal from simulated mine effluents. *Sep. Purif. Technol.* **2024**, *329*, 125168. [CrossRef]
12. Jiang, M.; Fang, Z.; Liu, Z.; Huang, X.; Wei, H.; Yu, C.Y. Application of membrane distillation for purification of radioactive liquid. *Clean. Eng. Technol.* **2023**, *12*, 100589. [CrossRef]
13. Mittal, H.; Alfantazi, A.M.; Alhassan, S.M. Recent developments in the adsorption of uranium ions from wastewater/seawater using carbon-based adsorbents. *J. Environ. Chem. Eng.* **2023**, *12*, 111705. [CrossRef]
14. Wu, Y.; Chen, D.; Kong, L.; Tsang, D.C.W.; Su, M. Rapid and effective removal of uranium (VI) from aqueous solution by facile synthesized hierarchical hollow hydroxyapatite microspheres. *J. Hazard. Mater.* **2019**, *371*, 397–405. [CrossRef]
15. Chen, T.; He, P.; Liu, T.; Zhou, L.; Li, M.; Yu, K.; Meng, Q.; Lian, J.; Zhu, W. MXene-derived 3D defect-rich TiO_2@ Reduced graphene oxide aerogel with ultrafast carrier separation for photo-assisted uranium extraction: A combined batch, X-ray absorption spectroscopy, and density functional theory calculations. *Inorg. Chem.* **2022**, *61*, 12759–12771. [CrossRef]
16. Shen, C.J.; Pan, J.Q.; Chen, M.L.; Su, M.H.; Chen, D.Y.; Song, G. Statistically and visually analyzing the latest advancements and future trends of uranium removal. *Environ. Res.* **2023**, *239*, 117280. [CrossRef]

17. Wang, W.; Wang, Z. Magnetic $NiFe_2O_4$@SiO_2@CS-PBTCA nanoparticles for uranium adsorption. *J. Radioanal. Nucl. Chem.* **2023**, *332*, 5007–5016. [CrossRef]
18. Li, H.; Li, L.; Wen, J.; Ye, G.; Chen, J.; Wang, X. Introducing self-assembly effect in adsorption process for efficient uranium extraction by zwitterion highly-functionalized fibers. *Chem. Eng. J.* **2023**, *456*, 140935. [CrossRef]
19. Yang, A.; Wang, Z.; Zhu, Y. Facile preparation and adsorption performance of low-cost MOF@ cotton fibre composite for uranium removal. *Sci. Rep.* **2020**, *10*, 19271. [CrossRef]
20. Li, N.; Zhou, L.; Jin, X.; Owens, G.; Chen, Z. Simultaneous removal of tetracycline and oxytetracycline antibiotics from wastewater using a ZIF-8 metal organic-framework. *J. Hazard. Mater.* **2019**, *366*, 563–572. [CrossRef]
21. Zhou, L.; Li, N.; Owens, G.; Chen, Z. Simultaneous removal of mixed contaminants, copper and norfloxacin, from aqueous solution by ZIF-8. *Chem. Eng. J.* **2019**, *362*, 628–637. [CrossRef]
22. Troyano, J.; Carné-Sánchez, A.; Avci, C.; Imaz, I.; Maspoch, D. Colloidal metal–organic framework particles: The pioneering case of ZIF-8. *Chem. Soc. Rev.* **2019**, *48*, 5534–5546. [CrossRef]
23. Schejn, A.; Balan, L.; Falk, V.; Aranda, L.; Medjahdi, G.; Schneider, R. Controlling ZIF-8 nano-and microcrystal formation and reactivity through zinc salt variations. *CrystEngComm* **2014**, *16*, 4493–4500. [CrossRef]
24. Lee, Y.R.; Jang, M.S.; Cho, H.Y.; Kwon, H.J.; Kim, S.; Ahn, W.S. ZIF-8: A comparison of synthesis methods. *Chem. Eng. J.* **2015**, *271*, 276–280. [CrossRef]
25. Lai, L.S.; Yeong, Y.F.; Lau, K.K.; Azmi, M.S. Fast synthesis of highly crystalline ZIF-8 using microwave-assisted solvothermal method. *Appl. Mech. Mater.* **2015**, *773*, 1133–1137. [CrossRef]
26. Taheri, M.; Bernardo, I.D.; Lowe, A.; Nisbet, D.R.; Tsuzuki, T. Green full conversion of ZnO nanopowders to well-dispersed zeolitic imidazolate framework-8 (ZIF-8) nanopowders via a stoichiometric mechanochemical reaction for fast dye adsorption. *Cryst. Growth Des.* **2020**, *20*, 2761–2773. [CrossRef]
27. Ma, S.; Leung, K.M.; Liao, C.; Chang, C.K.; Zhou, Y.; Chen, S.; Zhao, X.; Zhao, Q.; Shih, K. Green conversion of waste alkaline battery material to zeolitic imidazolate framework-8 and its iodine capture mechanism. *J. Hazard. Mater.* **2024**, *469*, 133612. [CrossRef] [PubMed]
28. Luo, K.; Wang, Q.; Xin, Q.; Lei, Z.; Hu, E.; Wang, H.; Liang, F.; Wang, H. Uranium adsorption properties and mechanism of ZIF-8/microalgae composite adsorbent with crosslinked chitosan/tannic acid curing supported by quaternary phosphate ionic liquid. *Desalination* **2024**, *592*, 118079. [CrossRef]
29. Wu, J.; Shi, N.; Li, N.; Wang, Z. Dual-ligand ZIF-8 bearing the cyano group for efficient and selective uranium capture from seawater. *ACS Appl. Mater. Interfaces* **2023**, *15*, 46952–46961. [CrossRef] [PubMed]
30. Zeng, Y.; Liu, S.; Xu, J.; Zhang, A.; Song, Y.; Yang, L.; Pu, A.; Ni, Y.; Chi, F. ZIF-8 in-situ growth on amidoximerized polyacrylonitrile beads for uranium sequestration in wastewater and seawater. *J. Environ. Chem. Eng.* **2021**, *9*, 106490. [CrossRef]
31. Tuo, K.; Li, J.; Li, Y.; Liang, C.; Shao, C.; Hou, W.; Li, Z.; Pu, S.; Deng, C. Construction of hierarchical porous and polydopamine/salicylaldoxime functionalized zeolitic imidazolate framework-8 via controlled etching for uranium adsorption. *Mater. Horiz.* **2024**, *11*, 3364–3374. [CrossRef]
32. Chang, X.; Hu, P.; Liu, H.; Lv, Z.; Yang, J.; Wang, J.; Li, Z.; Qian, L.; Wu, W. ZIF-8 modified graphene oxide/sodium alginate 3D elastic spheres for uranium trapping in seawater. *Desalination* **2023**, *549*, 116371. [CrossRef]
33. Kida, K.; Okita, M.; Fujita, K.; Tanaka, S.; Miyake, Y. Formation of high crystalline ZIF-8 in an aqueous solution. *CrystEngComm* **2013**, *15*, 1794–1801. [CrossRef]
34. Zhang, C.; Chen, W.; Owens, G.; Chen, Z. Recovery of rare earth elements from mine wastewater using alginate microspheres encapsulated with zeolitic imidazolate framework-8. *J. Hazard. Mater.* **2024**, *471*, 134435. [CrossRef]
35. Liu, J.; He, J.; Wang, L.; Li, R.; Chen, P.; Rao, X.; Deng, L.; Rong, L.; Lei, J. NiO-PTA supported on ZIF-8 as a highly effective catalyst for hydrocracking of Jatropha oil. *Sci. Rep.* **2016**, *6*, 23667. [CrossRef]
36. Zhang, Y.; Jia, Y.; Hou, L.A. Synthesis of zeolitic imidazolate framework-8 on polyester fiber for PM2.5 removal. *RSC Adv.* **2018**, *8*, 31471–31477. [CrossRef] [PubMed]
37. Kalam, S.; Abu-Khamsin, S.A.; Kamal, M.S.; Patil, S. Surfactant Adsorption Isotherms: A Review. *ACS Omega* **2021**, *6*, 32342–32348. [CrossRef]
38. Zhu, K.; Chen, C.; Wang, H.; Xie, Y.; Wakeel, M.; Wahid, A.; Zhang, X. Gamma-ferric oxide nanoparticles decoration onto porous layered double oxide belts for efficient removal of uranyl. *J. Colloid Interface Sci.* **2019**, *535*, 265–275. [CrossRef]
39. Liu, Y.; Huo, Y.; Wang, X.; Yu, S.; Ai, Y.; Chen, Z.; Zhang, P.; Chen, L.; Song, G.; Alharbi, N.S.; et al. Impact of metal ions and organic ligands on uranium removal properties by zeolitic imidazolate framework materials. *J. Clean. Prod.* **2021**, *278*, 123216. [CrossRef]

Disclaimer/Publisher's Note: The statements, opinions and data contained in all publications are solely those of the individual author(s) and contributor(s) and not of MDPI and/or the editor(s). MDPI and/or the editor(s) disclaim responsibility for any injury to people or property resulting from any ideas, methods, instructions or products referred to in the content.